Fused 3-Stage Image Segmentation for Pleural Effusion Cell Clusters

Sike Ma*, Meng Zhao*†, Hao Wang† , Fan Shi*, Xuguo Sun‡, Shengyong Chen*, Hong-Ning Dai§
*Key Laboratory of Computer Vision and System of Ministry of Education
School of Computer Science and Engineering, Tianjin University of Technology, Tianjin, China
†Department of Computer Science, Norwegian University of Science and Technology
‡School of Medical Laboratory, Tianjin Medical University
§Faculty of Information Technology, Macau University of Science and Technology, Macau
Emails: sike_ma@126.com, zh_m@tju.edu.cn, hawa@ntnu.no, shifan@email.tjut.edu.cn
sunxuguo@tmu.edu.cn, sy@ieee.org, hndai@ieee.org

***Abstract*—The appearance of tumor cell clusters in pleural effusion is usually a vital sign of cancer metastasis. Segmentation, as an indispensable basis, is of crucial importance for diagnosing, chemical treatment, and prognosis in patients. However, accurate segmentation of unstained cell clusters containing more detailed features than the fluorescent staining images remains to be a challenging problem due to the complex background and the unclear boundary. Therefore, in this paper, we propose a fused 3-stage image segmentation algorithm, namely Coarse segmentation-Mapping-Fine segmentation (CMF) to achieve unstained cell clusters from whole slide images. Firstly, we establish a tumor cell cluster dataset consisting of 107 sets of images, with each set containing one unstained image, one stained image, and one ground-truth image. Then, according to the features of the unstained and stained cell clusters, we propose a three-stage segmentation method: 1) Coarse segmentation on stained images to extract suspicious cell regions-Region of Interest (ROI); 2) Mapping this ROI to the corresponding unstained image to get the ROI of the unstained image (UI-ROI); 3) Fine Segmentation using improved automatic fuzzy clustering framework (AFCF) on the UI-ROI to get precise cell cluster boundaries. Experimental results on 107 sets of images demonstrate that the proposed algorithm can achieve better performance on unstained cell clusters with an F1 score of 90.40%.**

I. Introduction

Lung cancer is currently one of the most serious cancers in the world, which has the highest incidence and mortality rate among all human cancers [1]. Pleural effusion is a common complication of lung adenocarcinoma. Detection of tumor cell clusters in pleural effusion is one of the effective means to determine whether there is tumor metastasis from or to the lung [2], [3]. Pleural effusion tumor cell cluster segmentation is a crucial prerequisite for obtaining reliable morphological statistics. The unstained images (original images) normally have much more detailed features than the florescence stained images which may become key features for abnormal cell detection. However, due to the complex background and the unclear boundaries, accurate segmentation from unstained cell clusters remains a challenging problem.

In recent years, many researchers have done a lot of analytical research on various types of data [4], especially for cell pathology images [5]–[9]. The current cell segmentation algorithms can be roughly divided into cluster-based cell segmentation algorithms, graph-based cell segmentation algorithms, and threshold-based cell segmentation algorithms. In particular, Yurtsever et al. [10] proposed an extended k-means clustering algorithm to segment nuclei in colon images. The improved extended k-means clustering algorithm reduces the number of iterations required and shortens the duration of the segmentation process. Compared with the weighted k-means clustering algorithm, the extended k-means clustering algorithm based on some parameters performs better. Bai et al. [11] proposed a particle swarm algorithm (FOPSO) based on fractional-order velocity, which combined with the improved fuzzy c-mean (FCM) algorithm (SI-IFCM) to achieve accurate segmentation of cell images. The improved intuitive membership makes the direct membership closer to the cluster boundary between the background and the cells, thereby improving the robustness to intensity changes. Integrating local shape information into SI-IFCM and FOPSO improves the performance of the touch unit. The final FOPSO is optimized in combination with SI-IFCM to avoid local extremes and sensitivity to initialization. Nguyen et al. [12] proposed a graph theory technique to segment glands. In the image, a map of the nucleus and lumen was established, and the map was divided into different parts using a standardized cutting method, each part corresponding to a gland. Unlike most state-of-the-art lumen-based gland segmentation methods, the nucleus-based approach can segment glands without cavities or glands with multiple cavities. Zhang et al. [13] proposed a global and local segmentation method based on graph cut (GC) method to segment images containing healthy cells and abnormal cells. The proposed global GC method allows the cytoplasm to be described when the image histogram presents a non-bimodal distribution. The proposed local adaptive graph cut (LAGC) method and pit-based nuclear segmentation method can achieve nuclear segmentation in pathological images and overlapping cell images. For kernel segmentation, especially in the case of nuclear anomalies, they proposed an adaptive and localized graphics segmentation method that allows combining intensity, texture, boundary, and region information. Li et al. [14] proposed to use a double threshold method to segment white blood cells from acute lymphocyte whitening

and images. This method effectively combines the single-threshold segmentation method based on the RGB color space and the single-threshold segmentation method based on the HSV color space to achieve high segmentation accuracy.

Although there are many existing studies on cell segmentation, there are very few algorithms for pleural effusion cell cluster segmentation. In this paper, in order to accurately and quickly extract suspicious cell areas from tumor cell clusters, we propose a three-stage fusion segmentation algorithm namely Coarse segmentation-Mapping-Fine (CMF) segmentation. This method fuses the fluorescent staining information of the cells and retains the texture, morphology, and other information of the unstained image. Specifically, we address two *major problems* of tumor cluster segmentation:

1) The data acquisition and labelling of tumor cell clusters in pleural effusion are difficult.
   - We establish a dataset of cell clusters with ground truth, by collaborating with health professionals.
2) Existing cell recognition algorithms usually focus on the characteristics of individual cells, and tumor cell metastasis is more efficient than tumor cells when pleural effusion tumor cell clusters fall off into the blood. Tumor cell clusters suggest a worse prognosis.
   - We propose a fused segmentation algorithm **CMF** for cell clusters to obtain accurate segmentation boundaries.

The rest of the paper is organized as follows. The principle of the fusion algorithm and the establishment of a tumor cell dataset are introduced in Section II. The experimental results are shown and the segmentation results of pathological images of tumor cell clusters between different methods are compared and evaluated in Section III. The paper is concluded in Section IV.

II. Methodology

A. Dataset

We have established a dataset of pleural effusion tumor cell cluster images. To ensure the diversity of pleural effusion cell data, the dataset includes three groups: clinical group, simulation group, and cancer cell group (as depicted in Figure 1). The clinical group consists of 22 cases of pathological images obtained from the pleural effusion of lung cancer patients. The simulation group mixes A549 cells and blood cells into a cell suspension to simulate the pleural effusion of clinical lung cancer patients, in which a total number of 50 sample images are obtained. The cancer group refers to the sample that contains only A549 tumor cells. There are 35 samples in this group. In this group, the background of the cell image is relatively pure, and the cell area is highly distinguished from the background.

Therefore, a dataset with a total number of 107 sets of cell cluster images is established, within each set, there is an unstained (original) image, a fluorescent stained image, and a ground-truth image (as shown in Figure 1 where each column consisting of 3 images represents a set).

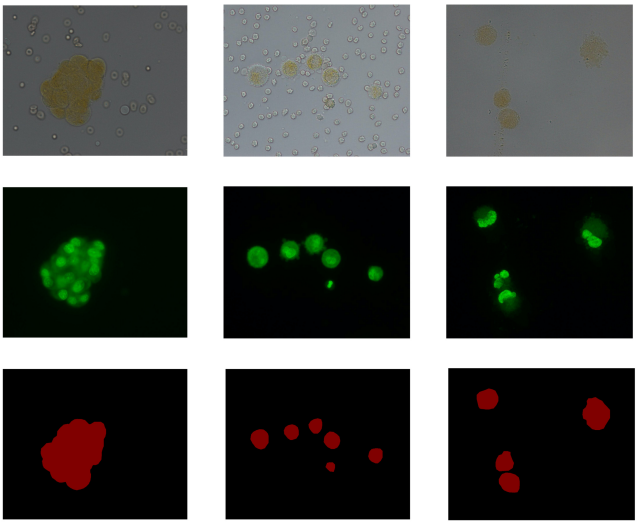

Fig. 1: Tumor cell clusters pathology image samples and their corresponding fluorescent staining images and the ground-truth images. In each sub-image, from the first row to the third row are the original image, fluorescent staining image, the ground truth (the cell area is marked in red). From left to right, the vertical columns are the clinical group, the simulation group, and the cancer cell group.

B. CMF

As observed from Figure 1, the original images contain more detailed features than the stained images, however, the presence of proteins, bacteria, and other non-cell impurities and the blurred boundaries makes it difficult to obtain accurate segmentation. In order to achieve more precise cell cluster boundaries from the original images, we propose CMF algorithm, as shown in Figure 2.

1) Coarse Segmentation: Fluorescent staining can eliminate the interference of surrounding non-cell impurities, marking the cell area as a green fluorescent signal, and the rest background is marked as black (as shown in the second row of Figure 1). Therefore, in the coarse segmentation stage, the fluorescence-stained image is subjected to the maximum inter-class variance method (OTSU algorithm) [15], [16] to determine the maximum variance between the cell area and the background in the cell image. As a threshold value, the binarization operation is performed on each pixel in the image. This algorithm has better noise immunity, which can effectively eliminate the noise interference of uneven image coloring. Then, both the morphological expansion and corrosion operation are used to smooth the segmentation edge to extract region of interest (ROI) of the suspicious cell area.

2) Pixel Mapping: After achieving the ROI of the stained image, the ROI is mapped to the corresponding unstained image to obtain the ROI of the unstained image (UI-ROI) according to (1). The UI-ROI is then achieved to realize the preliminary cell area segmentation.

$$O_{p(x,y)} = \begin{cases} 1 & p(x,y) \in F_r \\ 0 & p(x,y) \notin F_r \end{cases}, \tag{1}$$

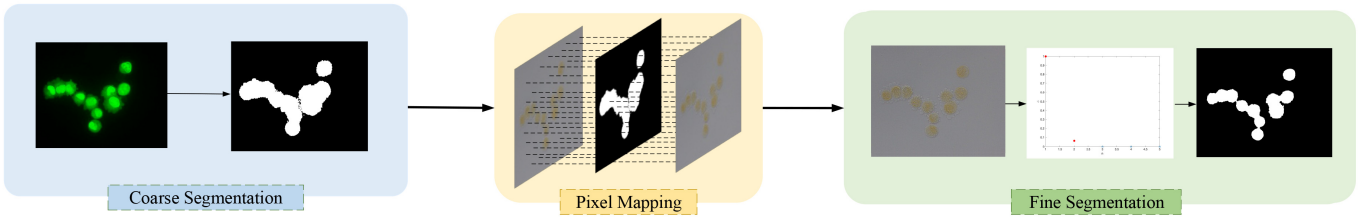

Fig. 2: Schematic overview of the proposed algorithm

where $O_{p(x,y)}$ is the cell for each pixel in the stained image and F_r is the ROI of the fluorescent stained image.

3) Fine Segmentation: It is considering that the sample image size in the dataset is 1280 × 1024, which belongs to a large-scale image and contains many pixels, which may lead to the problem of memory overflow. One of the advantages of the automatic fuzzy clustering framework segmentation framework (AFCF) [17] is that it can save memory consumption effectively by introducing hyper pixels. So the fine segmentation step is based on that which consists of three steps. The first step is the superpixel-based fast FCM algorithm (SFFCM) [18] for color image segmentation. The superpixel method, i.e., multiscale morphological gradient reconstruction (MMGR-WT) generates superpixel results for a color image to replace all pixels in the superpixel region with specific pixels to improve segmentation efficiency and to reduce the demand and consumption of hardware resources. According to (2), MMGR-WT requires two parameters: r_1 is the primary structural element denoted ,and η is the minimum threshold error represented .

$$J = \sum_{n=1}^{N} \sum_{\alpha=1}^{c} S_n R_{\alpha n}^{m} \left\| \left(\frac{1}{S_n} \sum_{\rho \in \theta_\rho} x_\rho \right) - k_\alpha \right\|^2, \qquad (2)$$

where N represents the total number of superpixel regions generated in the cell image, and the area of the n-th subregion is θ_ρ. The total number of pixels in this region is S_n, c is the total number of clusters, k_α represents the α-th cluster center, $R_{\alpha n}$ represents the α-th cluster, the fuzzy membership of the n-th superpixel sub-region, and $\mathcal{X}_\rho$ represents the cell image in each pixel.

The second step is the improved density peak algorithm (DP) with decision graph [19] based on the density balance algorithm to implement fully automatic clustering. The optimal cluster number is automatically generated by calculating the maximum interval in the decision graph. As shown in Figure 2, through calculation, the number of clusters in the sample image in the selected image is 2.

The third step is to obtain the final number of clusters and clustering results through the above steps. A prior entropy-based fuzzy clustering algorithm (PEFC) is used to obtain accurate cell cluster boundaries.

Algorithm 1 CMF

Input: Original graph and Fluorescent staining image
Output: Segmentation results

1: **/*Stage 1: Coarse Segmentation*/**
2: Otsu to divide the fluorescence stained image into regions of interest r_d and background m_d
3: Smooth segmentation results of expansion corrosion operation
4: **/*Stage 2: Pixel Mapping */**
5: Segmentation by comparing the pixel position of the original image
6: **for** each pixel (x, y) in original image do **do**
7: **if** fluorescent staining image (x, y) is in F_r **then**
8: mark the original drawing (x, y) in F_r
9: **else**
10: mark the original drawing (x, y) in F_m
11: **end if**
12: **end for**
13: **/*Stage 3: Fine Segmentation */**
14: MMGR-WT method to generate superpixel map of the result image obtained from Stage 2
15: Improved DP of the density balance algorithm to find the optimal number of clusters
16: PEFC algorithm to generate final segmentation result

$$J = \sum_{n=1}^{N} \sum_{\alpha=1}^{c} S_n R_{\alpha n} \Phi \left(\frac{1}{S_n} \sum_{\rho \in \theta n} x_\rho | k_\alpha, \Sigma_\alpha \right) + \sum_{n=1}^{N} \sum_{\alpha=1}^{c} S_n R_{\alpha n} \log \left(\frac{R_{\alpha n}}{T_\alpha} \right), \qquad (3)$$

where $\sum_\alpha$ represents the covariance matrix, and T_α is the prior probability that the superpixel region $\frac{1}{S_n} \sum_{\rho \in \theta n} x_\rho | k_\alpha$ belongs to k_α, which satisfies $0 \leq T_\alpha \leq 1$ and $\sum_{\alpha=1}^{c} T_\alpha = 1$.

4) CMF: The pseudo-code of the fused three stage segmentation algorithm for pleural effusion tumor cell clusters proposed in this paper is shown in Algorithm 1.

III. Experimental Results

The proposed CMF algorithm is completely self-adaptive, after all the parameters are set in advance, there will be no manual intervention needed during the experiments.According to our experiments, there are five parameters should be set

in advance. The recommended parameter combinations are as follows: the primary structural element denoted by r_1 is set to be 2, and the minimum threshold error represented by η is 10^{-5}, the weight index is set to 4, the minimum error threshold is set to 10^{-5}, and the maximum number of iterations is set to 100. This experiment runs on a computer with a 2.9 GHz, dual-core Intel Core i5 processor, 8 GB 1867 MHz DDR3 memory and MAC OS environment.

The proposed CMF algorithm for pleural effusion tumor cell cluster is implemented on the pleural effusion tumor cell dataset. In order to verify the effectiveness of the proposed algorithm, AFCF algorithm, adaptive morphological reconstruction segmentation algorithm (AMR) [20], Felzenszwalb and Hutten-locher's algorithm (EGB) [21] are compared qualitatively and quantitatively on three groups of cell images. The algorithm is evaluated with F1 score, Dice coefficient, and Jaccard coefficient.

A. Qualitative Analysis

Some examples of segmentation results with CMF for three groups of cell cluster images are shown in Figure 3. The three groups of results are clinical group, simulation group, and cancer cell group, respectively. For each cell image subpicture, the first row is the original cell picture, the second row is the ground truth labeled by the pathologist, the third row is the experimental result in this paper and the fourth row is the segmented cell area corresponding to the original image, which can not only locate the tumor cell area, but also carry multi-dimensional information such as color, texture, and morphology. For easy differentiation, in the ground truth row, the background is covered in black and the cell area is filled in red. In segmentation results, background is covered with black and the cell area generated by the segmentation algorithm is filled in white.The fifth row is another display of segmentation results. The red line is ground truth, and the blue line is the segmentation result of CMF algorithm.

In order to ensure the fairness of the comparison, we compare our CMF with the three aforementioned algorithms: AFCF, AMR, EGB (as shown in Figure 4).When there are many impurities around the cluster in the image, AFCF and EGB can not eliminate impurities' interference and can not define the outline of the cell cluster well. AMR's overall result is that it will over segment the cluster and lose much information. Besides, Figure 5 shows the segmentation results after adding coarse segmentation to various comparison algorithms, named AMR with coat segmentation (AMRCS) and EGB with coat segmentation (EGBCS). According to the segmentation results, We have found that the proposed CMF algorithm effectively excludes the effects of surrounding non-cell impurities in the segmentation of the three groups of cell images. It accurately distinguishes and locates tumor cell clusters' position and shows excellent performance in obtaining precise cell boundaries. Also, it proves the critical role of rough segmentation in the entire CMF algorithm.

To demonstrate the effectiveness of our proposed method, we validate CMF on a publicly available dataset BBBC020 [22] which consists of 20 fluorescence stained images. The segmentation results are shown in Figure 6. When the cell adhesion is severe, the CMF algorithm can segment the whole cell block area; when the cells are separated, the CMF algorithm can complete the segmentation of individual cells.

B. Evaluating Indicator

From the segmentation results, we can see that the AFCF algorithm and the EGB algorithm cannot be perform very well in the "clinical group" and "simulation group" on some complex and noisy cell images. AMRCS achieves too small segmentation areas, while segmentation areas of EGBCS are relatively too large. In comparison, the proposed CMF algorithm and the AMR algorithm can effectively obtain more accurate cell regions. However, for more precise boundaries of tumor cell clusters, the CMF algorithm outperforms all the other methods, which achieves accurate segmentation results in complex images.

To further demonstrate that the proposed CMF algorithm is suitable for tumor cell cluster segmentation, we evaluate the segmentation results on our 107 sets of images with a quantitative analysis, in which the F1 score, Dice coefficient, and Jaccard coefficient are used as the indicators.

In order to accurately define each evaluation index, in this paper, G is used to represent the actual value marked by the doctor, and R is the segmentation result. TP (True Positive) indicates the number of pixels in the cell area that is detected correctly, and FP (False Positive) indicates the number of pixels in the segmented cell area, which are the pixels in the cell area in Ground-Truth. FN (False Negative) indicates the number of pixels that are labeled as a cell region but are not detected in the segmentation in Ground-Truth, and TN (True Negative) indicates that it is not labeled as a cell region in the Ground-Truth and is also not detected in the segmentation result.

Then Precision and Recall are defined as follows, respectively:

$$\text{Precision} = \frac{TP}{TP + FP}, \tag{4}$$

$$\text{Recall} = \frac{TP}{TP + FN}. \tag{5}$$

Low Precision indicates that there are more false detection pixels, and Low Recall indicates that there are more missed pixels.

F1 score, also known as balanced f score, takes into account both accuracy and recall. It is defined as the harmonic average of the accuracy rate and recall rate. F1 score can be regarded as a weighted average of model accuracy and recall rate. Its maximum value is 1, and its minimum value is 0. The higher F1 score indicates the better performance of the algorithm. F1 score is defined as follows.

$$F1 = \frac{2 \times \text{Precision} \times \text{Recall}}{\text{Precision} + \text{Recall}}. \tag{6}$$

The Dice coefficient is a measure of the overlap between the segmentation result and the ground truth. The range is $[0, 1]$,

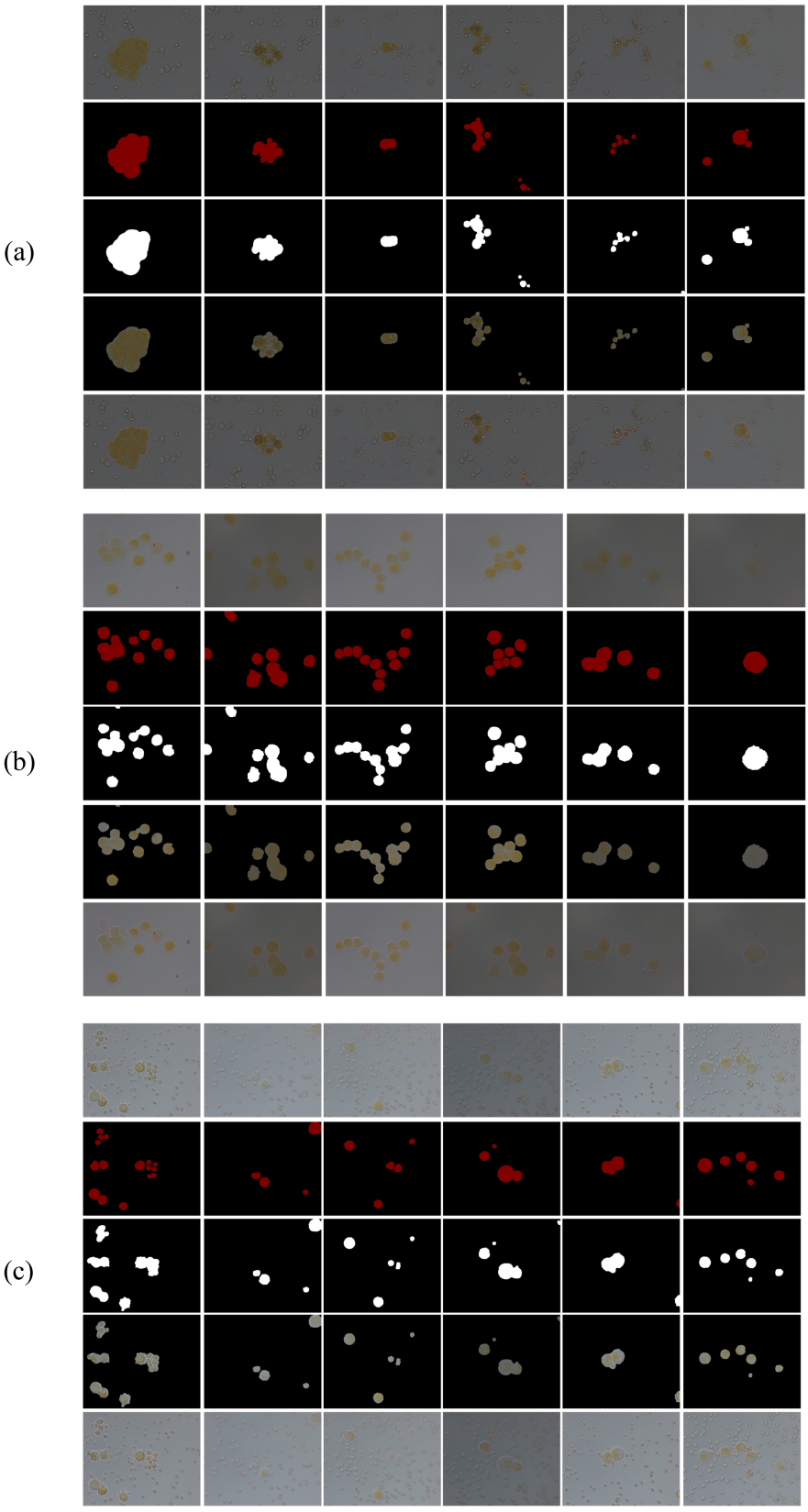

Fig. 3: Results of **CMF** algorithm on images in three groups. From top to bottom, (a) is the clinical group, (b) is the cancer cell group, and (c) is the simulation group. For each group, the first row: unstained images; the second row: ground-truth images; the third row: experimental results; the fourth row: segmentation results on unstained images;the fifth row: segmentation results.The red line is ground truth, and the blue line is the result of CMF segmentation.

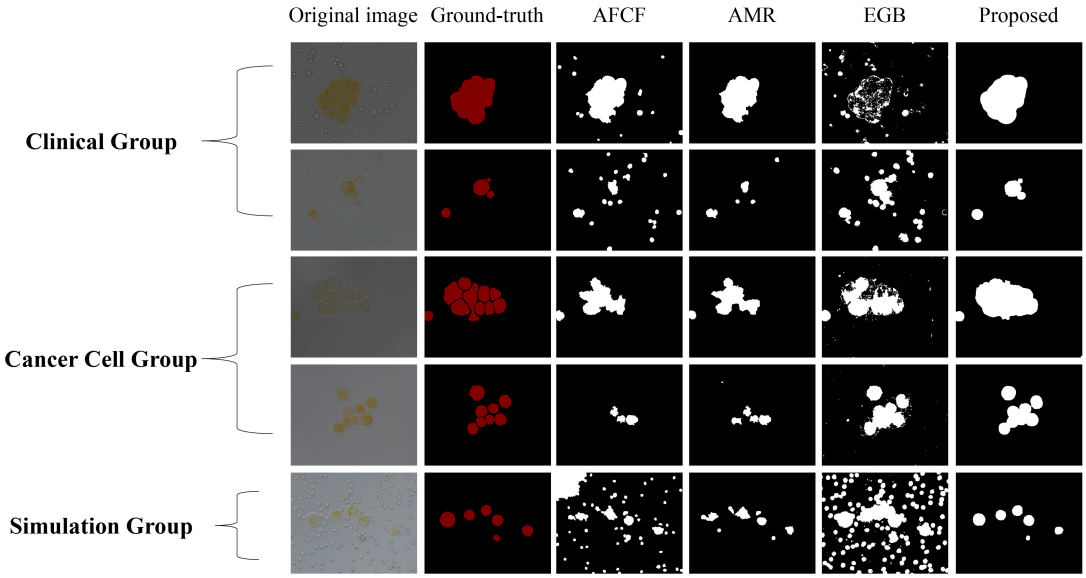

Fig. 4: Sample results obtained by applying AMR, EGB, AFCF and CMF algorithm to an image from the dataset

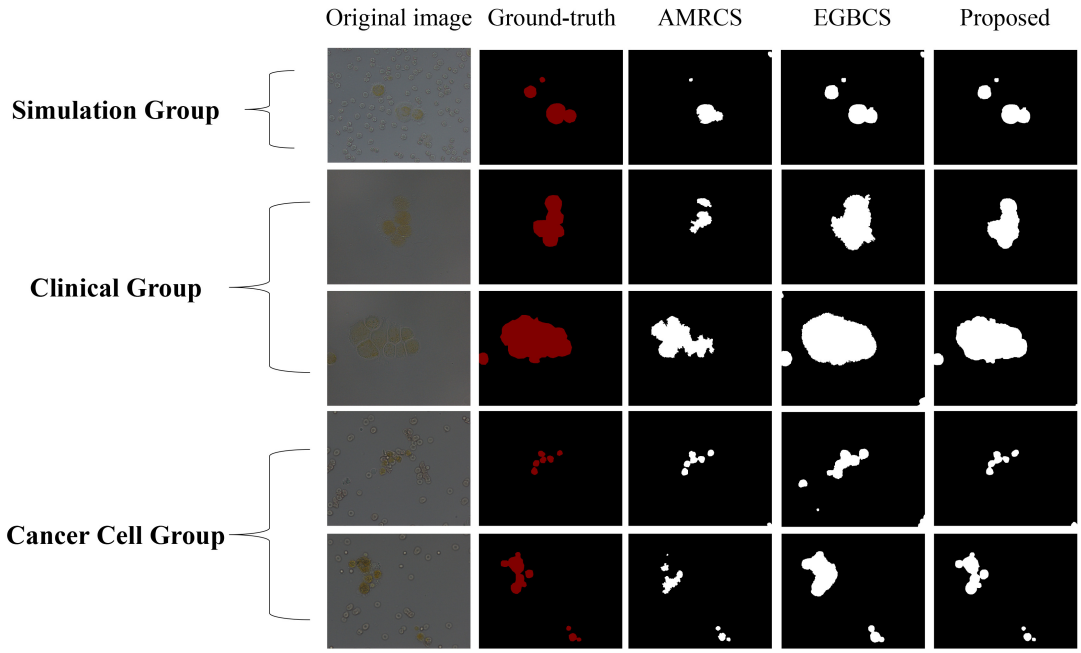

Fig. 5: Sample results obtained by applying AMRCS, EGBCS and CMF algorithm to an image from the dataset

which means from completely non-coincidence to completely coincidence. The calculation formula for the Dice coefficient is as follows:

$$\text{Dice}\left(G,R\right)=2\times\frac{G\cap R}{G+R}=2\times\frac{TP}{TP+FP+TP+FN}\ . \quad (7)$$

The Jaccard coefficient is defined as the ratio of the intersection and union of the segmentation result and the ground truth. The range is $[0,1]$. The larger the value of the Jaccard coefficient means the closer the model segmentation result to the standard segmentation result. The formula is as follows.

$$\text{Jaccard}=\frac{G\cap R}{G\cup R}=\frac{TP}{TP+FP+FN}. \quad (8)$$

C. Quantitative analysis

Table I shows the segmentation performance of all segmentation algorithms. Each of the three comparison algorithms (AFCF, AMR, EGB) has significantly improved the performance after adding the coarse segmentation steps. The algorithm without the coarse segmentation steps cannot locate the cells well, consequently failing to obtain the accurate

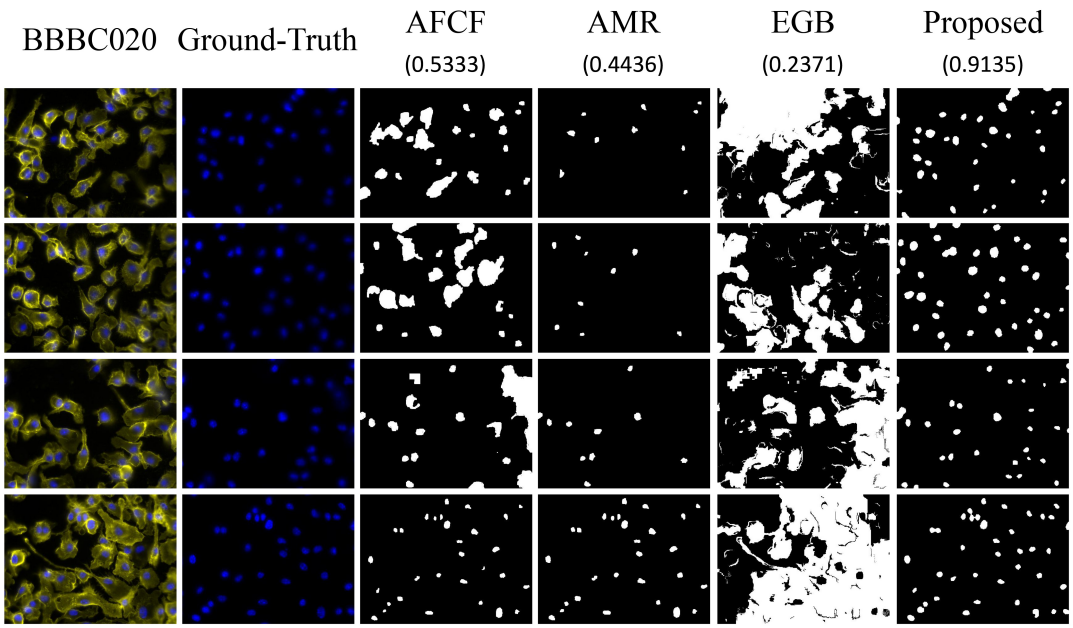

Fig. 6: Sample results obtained by applying AMRCS, EGBCS and CMF algorithm to an image from BBBC020.The Dice coefficient is shown in brackets

TABLE I: Comparison of all algorithms in the segmentation performance on cell cluster dataset

Group	Method	Dice	Jaccard	F1-score
The Simulation Group (50 sets)	AMR	0.4613	0.3057	0.4691
	EGB	0.5352	0.4028	0.6271
	AFCF	0.4478	0.3308	0.4642
	AMRCS	0.6388	0.4845	0.6693
	EGBCS	0.8175	0.7082	0.8385
	CMF	**0.8845**	**0.7957**	**0.8886**
The Cancer Cell Group (35 sets)	AMR	0.5015	0.3480	0.5081
	EGB	0.6140	0.4871	0.6958
	AFCF	0.5163	0.3688	0.5558
	AMRCS	0.6079	0.4568	0.6281
	EGBCS	0.8169	0.6918	0.8179
	CMF	**0.9250**	**0.8611**	**0.9263**
The Clinical Group (22 sets)	AMR	0.5394	0.3918	0.5503
	EGB	0.5494	0.4155	0.6338
	AFCF	0.6383	0.5154	0.6458
	AMRCS	0.7227	0.5952	0.7296
	EGBCS	0.7848	0.6689	0.8020
	CMF	**0.8961**	**0.8148**	**0.8972**

segmentation results. In the simulation group and the clinical group, there are many impurity cells in the image. After adding the coarse segmentation step, the segmentation effect will be increased by about 20%, and in the cancer cell group, the segmentation effect will be improved by more than 10%. As shown in Table I, we can find that the proposed CMF algorithm has achieved superior segmentation performance than other algorithms among all the groups in terms of accuracy and robustness.

IV. Conclusion

In this paper, we propose a new CMF algorithm for pleural effusion tumor cell cluster. With the help of fluorescence images, this method first obtains the ROI of the suspicious cell area, then mapping the ROI to the original image to get the UI-ROI, then, based on superpixel algorithm, the improved fuzzy clustering segmentation is combined with the density balance algorithm together wtih improved DP to obtain accurate cell cluster boundaries. Experimental results indicate that compared with the other segmentation methods, our method performs better on the three groups of images which consists of 107 sets of images, with an average F1 score of 90.40%, an average Dice of 90.18% and an average Jaccard of 82.38%.

Segmentation of pleural effusion tumor cell clusters is one of the critical pre-processing steps for diagnosis of lung ade-

nocarcinoma. However, single cell segmentation from clusters is still a tough problem. U-net [23], [24] is reported to be the most effective method for medical image segmentation, especially cell segmentation. Therefore, in the future, we are trying to combine deep learning methods such as U-net to separate the overlapping cells from the unstained pleural effusion cell clusters, and identify the normal cells and tumour cells, so as to determine the cancer severity of the patient.

ACKNOWLEDGMENT

This document is the results of the research project funded by the National Science Foundation of China (Grant Nos. 61703304, 61906133 and U1509207), R & D Plan in Key Field of Guangdong Province (Grant No. 2019B010109001), Major Science and Technology Projects of Tianjin (Grant No.18ZXZNGX00150) and is carried out with the support of ERCIM 'Alain Bensoussan' Fellowship Programme.

REFERENCES

[1] A. F. Sarioglu, N. Aceto, N. Kojic, M. C. Donaldson, M. Zeinali, B. Hamza, A. Engstrom, H. Zhu, T. Sundaresan, D. T. Miyamoto *et al.*, "A microfluidic device for label-free, physical capture of circulating tumor cell clusters," *Nature Methods*, vol. 12, no. 7, pp. 685–691, 2015.

[2] F. I. Bray, J. Ferlay, I. Soerjomataram, R. L. Siegel, L. A. Torre, and A. Jemal, "Global cancer statistics 2018: Globocan estimates of incidence and mortality worldwide for 36 cancers in 185 countries," *CA: A Cancer Journal for Clinicians*, vol. 68, no. 6, pp. 394–424, 2018.

[3] J. Yan, F. Shi, M. Zhao, Z. Wang, Y. Yang, and S. Chen, "Confocal raman sensing based on a support vector machine for detecting lung adenocarcinoma cells," *IEEE Sensors Journal*, vol. 19, no. 21, pp. 9624–9633, 2019.

[4] H.-N. Dai, H. Wang, R. Wong, and Z. Zheng, "Big data analytics for large scale wireless networks: Challenges and opportunities," *ACM Computing Surveys*, vol. (accepted to appear), 05 2019.

[5] A. Arbelle and T. R. Raviv, "Microscopy cell segmentation via adversarial neural networks," *arXiv: Computer Vision and Pattern Recognition*, 2017.

[6] J. Stegmaier, T. V. Spina, A. X. Falcao, A. Bartschat, R. Mikut, E. M. Meyerowitz, and A. Cunha, "Cell segmentation in 3D confocal images using supervoxel merge-forests with CNN-based hypothesis selection," pp. 382–386, 2018.

[7] A. Albayrak and G. Bilgin, "Automatic cell segmentation in histopathological images via two-staged superpixel-based algorithms," *Medical & Biological Engineering & Computing*, vol. 57, no. 3, pp. 653–665, 2019.

[8] A. Nedzved, S. Ablameyko, and I. Pitas, "Morphological segmentation of histology cell images," vol. 1, pp. 500–503, 2000.

[9] M. Zhao, A. Wu, J. Song, X. Sun, and N. Dong, "Automatic screening of cervical cells using block image processing," *Biomedical Engineering Online*, vol. 15, no. 1, pp. 14–14, 2016.

[10] U. Yurtsever, H. Evirgen, and M. C. Avunduk, "A New Augmented K-Means Algorithm for Seed Segmentation in Microscopic Images of the Colon Cancer," *Tehnički vjesnik*, vol. 25, no. 2, pp. 382–389, 2018.

[11] X. Bai, C. Sun, and C. Sun, "Cell Segmentation Based on FOPSO Combined With Shape Information Improved Intuitionistic FCM," *IEEE journal of biomedical and health informatics*, vol. 23, no. 1, pp. 449–459, 2018.

[12] K. Nguyen, A. Sarkar, and A. K. Jain, "Prostate cancer grading: Use of graph cut and spatial arrangement of nuclei," *IEEE Transactions on Medical Imaging*, vol. 33, no. 12, pp. 2254–2270, 2014.

[13] L. Zhang, H. Kong, C. T. Chin, S. Liu, Z. Chen, T. Wang, and S. Chen, "Segmentation of cytoplasm and nuclei of abnormal cells in cervical cytology using global and local graph cuts." *Computerized Medical Imaging and Graphics*, vol. 38, no. 5, pp. 369–380, 2014.

[14] Y. Li, R. Zhu, L. Mi, Y. Cao, and D. Yao, "Segmentation of white blood cell from acute lymphoblastic leukemia images using dual-threshold method," *Computational and Mathematical Methods in Medicine*, vol. 2016, pp. 9 514 707–9 514 707, 2016.

[15] R. Agrawal, S. Satapathy, G. Bagla, and K. Rajakumar, "Detection of white blood cell cancer using image processing," in *2019 International Conference on Vision Towards Emerging Trends in Communication and Networking (ViTECoN)*. IEEE, 2019, pp. 1–6.

[16] T. Bhagya, K. Anand, D. Kanchana, and A. A. Remya, "Analysis of image segmentation algorithms for the effective detection of leukemic cells," in *2019 3rd International Conference on Trends in Electronics and Informatics (ICOEI)*. IEEE, 2019, pp. 1232–1236.

[17] T. Lei, P. Liu, X. Jia, X. Zhang, H. Meng, and A. K. Nandi, "Automatic fuzzy clustering framework for image segmentation," *IEEE Transactions on Fuzzy Systems*, pp. 1–1, 2019.

[18] T. Lei, X. Jia, Y. Zhang, S. Liu, H. Meng, and A. K. Nandi, "Superpixel-Based Fast Fuzzy C-Means Clustering for Color Image Segmentation," *IEEE Transactions on Fuzzy Systems*, vol. 27, no. 9, pp. 1753–1766, 2019.

[19] A. Rodriguez and A. Laio, "Clustering by fast search and find of density peaks," *Science*, vol. 344, no. 6191, pp. 1492–1496, 2014.

[20] T. Lei, X. Jia, T. Liu, S. Liu, H. Meng, and A. K. Nandi, "Adaptive morphological reconstruction for seeded image segmentation," *IEEE Transactions on Image Processing*, vol. 28, no. 11, pp. 5510–5523, 2019.

[21] P. F. Felzenszwalb and D. P. Huttenlocher, "Efficient graph-based image segmentation," *International Journal of Computer Vision*, vol. 59, no. 2, pp. 167–181, 2004.

[22] V. Ljosa, K. L. Sokolnicki, and A. E. Carpenter, "Annotated high-throughput microscopy image sets for validation," *Nature Methods*, vol. 9, no. 7, pp. 637–637, 2012.

[23] T. Falk, D. Mai, R. Bensch, O. Cicek, A. Abdulkadir, Y. Marrakchi, A. Bohm, J. Deubner, Z. Jackel, K. Seiwald *et al.*, "U-Net: deep learning for cell counting, detection, and morphometry," *Nature Methods*, vol. 16, no. 1, pp. 67–70, 2019.

[24] Y. Li and L. Shen, "cC-GAN: A Robust Transfer-Learning Framework for HEp-2 Specimen Image Segmentation," *IEEE Access*, vol. 6, pp. 14 048–14 058, 2018.